DR. 70

ORNL/TM-6730

# Neutral Beam Energy and Power Requirements for Expanding Radius and Full Bore Startup of Tokamak Reactors

W. A. Houlberg
A. T. Mense
S. E. Attenberger



OAK RIDGE NATIONAL LABORATORY
OPERATED BY UNION CARBIDE CORPORATION · FOR THE DEPARTMENT OF ENERGY

## DISCLAIMER

Printed in the United States of America. Available from
National Technical Information Service
U.S. Department of Commerce
5285 Port Royal Road, Springfield, Virginia 22161
Price: Printed Copy ~~$5.25~~ 4.50; Microfiche $3.00

ORNL/TM-6730
Dist. Category UC-20 a, d, g

Contract No. W-7405-eng-26

FUSION ENERGY DIVISION

# NEUTRAL BEAM ENERGY AND POWER REQUIREMENTS FOR EXPANDING RADIUS AND FULL BORE STARTUP OF TOKAMAK REACTORS

W. A. Houlberg

A. T. Mense

S. E. Attenberger

Date Published - September 1979

**NOTICE** This document contains information of a preliminary nature. It is subject to revision or correction and therefore does not represent a final report.

Prepared by the
OAK RIDGE NATIONAL LABORATORY
Oak Ridge, Tennessee 37830
operated by
UNION CARBIDE CORPORATION
for the
DEPARTMENT OF ENERGY

THIS PAGE

WAS INTENTIONALLY

LEFT BLANK

CONTENTS

ABSTRACT

Neutral beam power and energy requirements are compared for full density full bore and expanding radius startup scenarios in an elongated plasma, The Next Step (TNS), as a function of beam pulse time and plasma density. Because of the similarity of parameters, the results should also be applicable to Engineering Test Facility (ETF) and International Tokamak Reactor (INTOR) studies. A transport model consisting of neoclassical ion conduction and anomalous electron conduction and diffusion based on "ALCATOR scaling" leads to average densities in the range $\langle n \rangle \sim 0.3\text{-}1.2 \times 10^{14}$ cm$^{-3}$ being sufficient for ignition. Neutral deuterium beam energies in the range 120-130 keV are adequate for penetration, with the required power injected into the plasma decreasing with increasing beam energy. The neutral beam power decreases strongly with increasing beam pulse length $t_b$ until $t_b$ exceeds a few total energy confinement times, yielding $t_b \simeq 4\text{-}5$ s for the TNS plasma. In addition to avoiding skin current effects and possibly allowing for a more impurity-free plasma initiation, the expanding radius scenario has slightly reduced beam energy and/or power requirements. When the expanding radius scenario is extended to even larger power reactors, a neutral deuterium beam energy of 150 keV remains sufficient for penetration.

# 1. INTRODUCTION

The startup of a tokamak reactor plasma can be divided into two general phases. First is an initiation phase in which global analyses have been used to obtain estimates for the applied toroidal voltage as a function of the neutral gas filling pressure [1-4]. The associated power requirements for ionization of the plasma have also been made with this type of analysis. Estimates of 60-150 V have been obtained for the required toroidal voltage in the Tokamak Fusion Test Reactor (TFTR) [3] with even higher estimates for reactors [4]. Microwave breakdown and preheating the electrons near the electron cyclotron and upper hybrid frequencies have been proposed as a means of reducing the peak voltage and power requirements during the initiation phase [5]. At the end of the first phase, there should be enough toroidal current in the plasma to produce closed magnetic flux surfaces and to provide a reasonable amount of ohmic heating to maintain the plasma. The analysis presented here concentrates on the second phase of startup, during which the plasma current, density, temperature, and size are brought to ignition conditions.

The one-dimensional (1-D) tokamak transport code WHIST is used to follow the evolution of density and temperature profiles in response to varying neutral beam energy and power levels. A brief summary of the physics models is presented in Section 2. A more thorough discussion of the equations and algorithms is contained in a companion report [6]. The models in the WHIST code are also discussed in work on the analysis

of thermal stability [7], the impact of poloidal divertors [8], and the effects of fueling profiles [9] in tokamak reactor plasmas.

In Section 3 a series of parameter surveys for startup of a TNS plasma is presented. These results should also be relevant for analyses of the tokamak ETF and studies of the IAEA-sponsored INTOR because of the similarity of machine parameters. Sensitivity to neutral beam energy, power, and injection time is examined. The effects of plasma density and limited variation in the transport model are also discussed for both full bore and expanding radius scenarios. The applicability of an expanding radius scenario to startup of a large power-producing tokamak is briefly presented in Section 4.

## 2. THE TRANSPORT MODEL

The 1-D fluid equations and physical models used in WHIST for this analysis are fully discussed in Ref. [6]. The 1-D fluid equations are those given by Hogan [10], but they have been generalized for multiple ion species in the manner presented by Hinton and Moore [11]; i.e., the energy balances for all thermal ion species are summed to obtain a single energy balance for all thermal ions at the same fluid temperature. The spatial differencing in the WHIST code conserves particles and energy on a nonuniform spatial mesh while the time differencing is treated implicitly to ensure the numerical stability of the stiff equations [12].

The plasma is divided into two radial zones: a plasma zone in which the magnetic field lines form closed magnetic surfaces and a scrape-off zone in which field lines connect to a material limiter or magnetic divertor. In the plasma zone, the multispecies particle and energy fluxes of Hinton and Moore [11] are used as the basis for neoclassical transport in the banana/plateau regime. In addition to the neoclassical expressions, anomalous contributions are added to the particle and electron heat fluxes with a diagonal model, i.e.,

$$Q_j = C_0 Q_j^{nc}$$

$$Q_e = Q_e^{nc} - n_e \chi_e^{an} \frac{\partial T_e}{\partial r}$$

$$\Gamma_j = \Gamma_j^{nc} - D^{an} \frac{\partial n_j}{\partial r}$$

$$\chi_e^{an} = \frac{C_1}{n(cm^{-3})} \ cm^2/s$$

$$D^{an} = C_2 \chi_e \ cm^2/s$$

where $C_0 = 1$, $C_1 = 5.25 \times 10^{17}$, and $C_2 = 0.2$ are used in this analysis unless otherwise noted. The subscripts j and e designate ion and electron species, respectively. Estimating $\chi_e$ from global electron energy confinement with the relation $\tau_{Ee} \simeq (a^2/4\chi_e)$ gives values of $C_1$ in the range $3\text{-}7 \times 10^{10}$ for ALCATOR [13], the Impurity Study Experiment (ISX-A) [14], and the Princeton Large Torus (PLT) [15] ohmically heated plasmas. The inverse density dependence of $\chi_e$ gives improved electron

energy confinement with increasing density, as has been shown experimentally. Further improvement in electron energy confinement with increasing temperature has been suggested in neutral-beam-heated PLT plasmas [16] but has not been incorporated into this analysis.

The model of Mense and Emmert [8] is used for transport in the scrape-off zone. Radial diffusion and electron and ion conduction are all assumed to be Bohm-like:

$$D = \chi_e = \chi_i = \frac{1}{15} \frac{kT_e}{eB}$$

Particle and energy losses due to flow along the magnetic field lines are evaluated self-consistently in terms of parallel flow rates and the buildup of a sheath potential at the limiter/collector plate. The characteristic distance along a field line that a particle must travel before being intercepted by the limiter/collector plate is evaluated from the magnetic field topology. For a wide scrape-off zone, the solution of the particle and energy equations in the plasma is insensitive to the boundary conditions applied at the chamber wall because radial flow of particles and energy from the plasma is balanced mostly by parallel flow loss in the scrape-off zone.

The ionization probability of wall-emitted impurities is typically very high in the scrape-off zone for the startup calculations presented in Section 3. In a 15-cm scrape-off zone, the typical ionization probabilities of 20-eV carbon, oxygen, and iron emitted isotropically from the wall are 99.3%, 99.6%, and ~100%, respectively. Thus, if the plasma is kept free of impurities during the breakdown phase and the divertor efficiently collects the impurities ionized in the scrape-off zone, the plasma should remain clean. The calculations presented in Section 3 presume impurity-free operation during the entire startup phase. Radiation losses are essentially due to hydrogenic bremsstrahlung and ionization of the neutral hydrogen gas. A limited amount of low-Z impurities should not affect the results significantly because they would become fully ionized during the beam-heating phase. However, high-Z impurities must be avoided.

Because the scrape-off zone is very wide, the ionization probability of neutral hydrogen is also very high in the scrape-off zone. For the same case presented above, the ionization probability of neutral hydrogen of 5 eV emitted isotropically from the wall is 88% in the scrape-off zone. Thus, gas puffing from the wall would put a very high particle load on the divertor and would also be a very inefficient fueling method. In the expanding radius scenarios (fixed major radius, increasing minor radius in this analysis), the scrape-off layer is even wider than that for the full bore scenarios cited above. In some cases essentially no wall-emitted neutrals reach the plasma before being ionized. For this reason we specify a source of neutral gas at the limiter radius in our expanding radius scenario; i.e., we require a

material limiter. Other alternatives would be to use pellet injection to penetrate the cold scrape-off layer or expand the plasma off the inside or outside wall of the chamber (vary the major radius simultaneously with the minor radius). SPUDNUT [17] is used to calculate the neutral gas fueling profiles with the source at the wall in full bore scenarios and at the limiter position in expanding radius scenarios.

Because neutral beam deposition calculations are a critical part of beam-heating analyses, the deposition profiles for the routine BEAM used in WHIST were benchmarked against FREYA (Monte Carlo-Princeton Plasma Physics Laboratory) [18] and HOFR (analytic-ORNL) [19] routines. The benchmark calculations showed excellent agreement for varying beam injection angle, energy, plasma size, and finite beam size in plasmas with circular cross sections [20]. BEAM has approximate corrections for noncircular geometry and flux surface shifts at high $\beta$, but these effects were not included in the benchmark calculations because of the lack of available codes at the time. A version of FREYA has since been modified to incorporate the effects of noncircular plasmas and flux surface shifts [21]. In all of the calculations presented in Sections 3 and 4, we use near-perpendicular injection ($12^{\circ}$ from perpendicular) in the plasma midplane with a beam radius of 12 cm. Only deposition of the full energy component is considered, and all powers refer to the power in the full energy component delivered to the plasma.

Faraday's and Ohm's laws are combined to obtain a current diffusion equation. Neoclassical resistivity is used even though this results in the formation of skin currents if the current ramp is strong enough during startup and the plasma radius is fixed. The expanding radius scenario reduces or eliminates skin current formation, as suggested by Düchs et al. [22]. In our opinion the lack of a skin current in experiments is more likely due to redistribution of current by magnetohydrodynamic (MHD) tearing mode activity [23-24] than to anomalous parallel resistivity. The elimination of skin currents during startup with a moving limiter, then, does not necessarily reduce resistive volt-second requirements but does reduce contact between the plasma and limiter during disruptive redistribution of skin currents; therefore, it should reduce the potential for contamination of the plasma during startup.

In all of our calculations, the spatial grid is fixed in time. When the calculations indicate that the prescribed movement of the limiter/separatrix has passed a spatial zone, the parallel loss terms are removed from that spatial zone, and a skin current element is added in accordance with the prescribed rate of current rise. In this way the plasma zone is increased in size stepwise, and there is a corresponding stepwise increase in the total plasma current. Illustrations of the algorithm are contained in Ref. [6]. For the calculations of Sections 3 and 4, the current is ramped linearly in time and the radius expanded in such a way that the safety factor q at the limiter remains constant. This is similar to the constant-of-expansion model of Düchs et al. [22] and Girard et al.

[25], although MHD analysis may dictate that greater shear is desirable. Some current diffusion occurs during the expansion phase such that shear is gradually introduced even though q at the limiter is constant in time.

## 3. NEUTRAL BEAM ENERGY AND POWER REQUIREMENTS FOR AN IGNITION DEVICE

The physical dimensions and parameters of the ignition-sized plasma shown in Table I are those of the Oak Ridge TNS design. The toroidal magnetic field for this study is 4.2 T, although it is higher in the base TNS design [26]. The startup results presented here are insensitive to the toroidal magnetic field but are somewhat more sensitive to the toroidal current because of the neoclassical ion conduction model. A higher magnetic field does, however, provide a greater margin for MHD beta limits.

The full bore scenario calculations start with a cold plasma at full density, toroidal current, and size. The expanding radius calculations start with half the final plasma radius (i.e., one quarter of the final plasma volume) and 1 MA of toroidal current. The current is increased linearly in time to 4 MA over the same time interval during which the neutral beams are applied. Hence, $t_b$ is used to denote both the expansion time and beam-heating time. The radius is also increased during $t_b$, such that the cross-sectional area increases linearly in time. The current density is added uniformly, and because of the choice of initial and final sizes and currents, the safety

factor q remains constant at the limiter. As the plasma is increased in size, the average plasma density is maintained by the neutral beams and the addition of cold fuel via gas puffing at the limiter. Only the full energy component of the beam is used so the impact of varying beam energy can be clarified. The beam power is the power delivered to the plasma and thus does not include neutralization efficiency. In fact, the extracted (preneutralization) power requirements may increase with increasing energy [27].

Figure 1 illustrates the impact of neutral beam energy on the peak and average ion temperatures for full bore and expanding radius scenarios after 1.5 s of heating. In all cases the total amount of energy injected is 90 MJ. As the beam energy is increased, the average ion temperature increases slightly. This indicates that the total energy content of the plasma at the end of the heating phase becomes higher when higher beam energies are used. The peak ion temperature increases more rapidly than the average, showing that the beam deposition becomes more centrally peaked as the beam energy is raised. The more peaked beam deposition and ion temperatures lead to longer confinement of the energy. None of these cases are near enough to ignition for alpha heating to be significant. The expanding radius cases are only slightly hotter than the full bore cases, indicating a modest increase in the heating efficiency for the expanding radius cases for a given beam energy. On the other hand, a somewhat lower beam energy could be used for the expanding radius scenario to achieve the same final plasma conditions as in the full bore scenario. The

better penetration in the initially small plasma is offset somewhat by a decrease in the confinement time because of the smaller size.

Because injection is nearly perpendicular to the magnetic axis (in the "co" direction), the beam path intersects the wall after one pass through the plasma. Figure 2 shows the fraction of the beam that passes entirely through the plasma without being ionized. Setting a constraint on the maximum allowable neutral beam flux on the inside wall sets an upper limit on the allowable neutral beam energy for a given plasma density. The small initial size for the expanding radius scenario allows 10% of a 150-keV $D^o$ beam to penetrate to the inside wall when the volume-averaged plasma density is $\langle n \rangle = 3 \times 10^{13}$ $cm^{-3}$. As the plasma radius is doubled, this loss drops to 0.5%. If the initial plasma density is even lower because of either the attractiveness of low density startup or physical limitations on the achievable density, neutral deuterium beam energies greater than 150-keV $D^o$ become unacceptable for near perpendicular injection in the expanding radius scenario. Beam orientation tangential to the inside wall of the torus is traditionally used to help prevent overpenetration of the beams in low density plasmas in addition to reducing orbit losses. Fast ion orbit losses in this device should be small [27]. For the remainder of this study, we use 120-keV $D^o$ beams for the expanding radius scenarios and 150-keV $D^o$ beams for the full bore scenarios. Examination of Fig. 1 shows that these two scenarios have equivalent heating efficiencies.

Low density startup scenarios have been proposed as a means of reducing beam energy and power requirements, but these scenarios have their greatest success if confinement losses decrease with decreasing plasma density as with classical or pseudoclassical transport models [25, 23]. Figure 3 shows that the peak and average ion temperatures required for ignition increase sharply at low plasma density because of the anomalous increase in electron conduction and convection losses at low density. Plasmas with volume-averaged density at the end of the heating phase of $\langle n \rangle \leq 7 \times 10^{13}$ cm$^{-3}$ will not ignite no matter how hot they are when the beams are shut off. It must be emphasized that this cutoff is sensitive to variations in the transport models. Ignition is defined by turning off the beam heating and observing whether the plasma quenches itself or manages to sustain itself on energy input from the fusion-produced alphas. The temperatures shown in Fig. 3 are characteristic values of both full bore and expanding radius scenarios at the time the beams are turned off. The density at the end of the heating phase may be reached by ramping from some lower value ($\langle n \rangle \leq 5 \times 10^{13}$ cm$^{-3}$) while heating the plasma. This could possibly reduce beam energy and/or power requirements [27, 29].

Perhaps the strongest controllable influence on the beam power required to heat a plasma to ignition is the beam pulse length [28]. Figure 4 shows the power in the full energy component needed to reach ignition in a given time for volume-averaged densities in the range $\langle n \rangle = 0.8\text{-}1.2 \times 10^{14}$ cm$^{-3}$ for a full bore startup. For very short startup times, confinement losses become negligible, and the stored energy of the plasma must be attained with higher power pulses such

that $P_b \propto t_b^{-1}$ (see Fig. 5). For very long startup times, confinement losses dictate a minimum power that must be supplied in order to reach ignition. The total energy supplied during the pulse then increases $\propto t_b$, as shown in Fig. 5. The total energy confinement time for these cases is in the vicinity of 1.5 s. Once the beam pulse length exceeds a few times the total energy confinement time, the beam power requirements are essentially reduced to an asymptotic level.

Note that the power required for ignition, as shown in Fig. 4, is fairly insensitive to the plasma density. This is further illustrated in Fig. 6. At very low plasma density, the increase in anomalous electron conduction and convection losses and the decrease in the fusion rate lead to an increase in the power required to reach the ignition temperature. For $\langle n \rangle \leq 1 \times 10^{13}$ cm$^{-3}$ with the base transport model, neither full bore nor expanding radius cases would ignite. At the higher end of the densities examined, beam penetration is reduced, and there is simply more plasma to heat. These two effects are not offset by the reduction in the anomalous losses. Also shown in Fig. 6 are some individual cases where the coefficients of the transport model were varied. With the modest variation shown here, the beam power can vary from $P_b$ = 35-80 MW. If the anomalous losses continue to decrease with increasing electron temperature as indicated by PLT beam-heating experiments [16], the power requirements are expected to lie at the lower end of this range.

The expanding radius cases with $E_b$ = 120 keV and the full bore cases with $E_b$ = 150 keV have essentially identical power requirements, a fact which is further illustrated in Fig. 7. If the beam energy is reduced to 120 keV for the full bore case, the power requirement is increased in agreement with the scaling $E_b \cdot P_b \approx$ constant shown analytically by Scott and Sheffield [30] and also numerically by Holmes et al. [27].

The beam deposition profiles for all of these scenarios are peaked on the magnetic axis. The beam energy deposition per unit plasma volume, denoted by H(r), is shown in Fig. 8 for a typical expanding radius scenario with $E_b$ = 120 keV and $\langle n \rangle = 10^{14}$ cm$^{-3}$. The beams are turned on in the interval $0.5 \leq t \leq 4.5$ s, and the plasma minor radius is doubled in size. The deposition profile goes from very strongly peaked on axis to only moderately peaked as the plasma reaches full size. Figure 9 illustrates the evolution of current profile for this same case. During the first 0.5 s, the plasma current is ramped to 1 MA while the plasma radius is maintained constant (a = 62.5 cm). A noticeable skin current develops because of the neoclassical model for resistivity. As mentioned earlier, resistive tearing mode activity would effectively redistribute this skin current [23, 24]. As the plasma is expanded to full size, toroidal current is added at the surface and essentially frozen into the plasma by the beam heating.

## 4. EXPANDING RADIUS STARTUP OF A LARGE TOKAMAK REACTOR

Girard et al. [25] applied their expanding radius analysis to large systems with a scenario very similar to the one presented in Section 3 of this report; i.e., the expansion and heating phases were simultaneous. For a machine with only a relatively modest margin for ignition, the full size must be reached by the end of the heating phase. However, in an expanding radius scenario for a much larger device, the beam heating phase may be terminated before the full size is reached, and a much more dramatic reduction in beam energy and power requirements can be realized.

A startup scenario based on this principle is shown in Fig. 10. In Phase I the plasma is initiated in some small region of the torus, and the current is ramped to an appropriate level determined by the desired safety factor q. In Phase II the size and current are increased simultaneously to avoid skin currents, and some heating is applied to reduce resistive volt-second losses and freeze in the current profile. At the end of this phase, an ignition-sized plasma is attained, i.e., one that meets the criteria of having enough current to confine fast alpha particles and is large enough to ignite. During Phase III neutral beams are turned on to heat the plasma to ignition. Finally, after the beams are turned off, excess fusion power from the core is used to heat cold plasma at the edge while the size and current are ramped to their final states.

This scenario was tested with the machine parameters shown in Tables II and III. The dimensions are essentially doubled from those for TNS given in Table I. The neutral beam energy was chosen to be the same as that for the full bore startup scenarios in Section 3, i.e., $E_b$ = 150 keV.

The plasma ignited easily with $P_b$ = 130 MW applied for 4 s during Phase III. The higher power requirement is due to the much larger plasma volume in this device compared to the TNS plasma and could probably be reduced with a longer beam pulse. Figure 11 shows that as the limiter is withdrawn during Phase IV, the conduction and convection losses from the plasma core heat the cold fuel added at the plasma edge.

If control of an expanding radius scenario is feasible, it can be used to great advantage in a large power reactor: the neutral beam energy required does not increase beyond that for an ignition device such as TNS/ETF/INTOR.

## 5. SUMMARY

Neutral deuterium beam energies in the range $E_b$ = 120-150 keV provide sufficient penetration for startup of an ignition-sized plasma if beam orientation is nearly perpendicular to the magnetic axis and average plasma densities are limited to $\langle n \rangle \approx 0.8\text{-}1.2 \times 10^{14}$ cm$^{-3}$ during startup. In addition to reducing the potential for skin current formation during startup, an expanding radius scenario allows a modest

reduction in beam energy without sacrificing beam penetration. Beam pulse time of the order of several energy confinement times minimizes beam power requirements for startup. An expanding radius scenario may hold its greatest promise for startup of a very large power reactor: beam energy requirements may not need to be increased beyond the energy required for startup of an ignition-sized device.

As this report was in its final preparation, an additional and possibly pessimistic effect on beam power requirements came to our attention from two separate sources [31, 32]. We have used a classical model for deposition of the fast alpha energy in the ion and electron fluids. At roughly the ignition temperature, the coupling between ions and electrons becomes weak, and the ions essentially allow the plasma to ignite by decoupling from the lossy electron channel. If alpha energy deposition in the electron fluid is anomalously high, it can be much more difficult to ignite the plasma [31] while anomalous transfer of alpha energy to the ion fluid can greatly reduce power requirements [32]. Even if the thermalization is classical, alphas may become trapped in the toroidal field ripple and drift out of the plasma before becoming completely thermalized. Because most of the energy transfer to the ion fluid occurs at the end of the alpha particle thermalization, the ion fluid suffers a proportionally greater energy loss than the electron fluid [33].

## ACKNOWLEDGMENTS

The authors would like to thank J. D. Callen, H. H. Haselton, J. T. Hogan, J. A. Holmes, H. C. Howe, G. G. Kelley, J. A. Rome, Y-K. M. Peng, N. A. Uckan, and R. M. Wieland for many fruitful discussions during the development of this work.

## REFERENCES


[1] ABRAMOV, V. A., POGUTSE, O. P., YURCHENKO, E. I., Sov. J. Plasma Phys. 1 (1975) 297.

[2] PAPOULAR, R., Nucl. Fusion 16 (1976) 37.

[3] HAWRYLUK, R. J., SCHMIDT, J. A., Nucl. Fusion 16 (1976) 775.

[4] ABRAMOV, V. A., VIKHREV, V. V., POGUTSE, O. P., Sov. J. Plasma Phys. 3 (1977) 288.

[5] PENG, Y-K. M., BOROWSKI, S. K., KAMMASH, T., Nucl. Fusion 18 (1978) 1439.

[6] MENSE, A. T., HOULBERG, W. A., ATTENBERGER, S. E., A 1-D Transport Model for Analysis of Expanding Radius and Full Bore Startup of Tokamak Reactors, Oak Ridge National Laboratory Rep. ORNL/TM-6841 (1979).

[7] HOULBERG, W. A., CONN, R. W., Nucl. Fusion 19 (1979) 81.

[8] MENSE, A. T., EMMERT, G. A., Nucl. Fusion 19 (1979) 361.

[9] MENSE, A. T., HOULBERG, W. A., ATTENBERGER, S. E., MILORA, S. L., "Effects of Fueling Profiles on Plasma Transport," to be published in Nucl. Fusion.

[10] HOGAN, J. T., "Multifluid Tokamak Transport Models," Methods in Computational Physics, Vol. 16 (KILLEEN, J., ALDER, B., FERNBACH, S., ROTENBERG, M., Eds) Academic Press, New York (1976) 131.

[11] HINTON, F. L., MOORE, T. B., Nucl. Fusion 14 (1974) 539.

[12] HOULBERG, W. A., CONN, R. W., Nucl. Sci. Eng. 64 (1977) 141.

[13] GONDHALEKAR, A., GRANETZ, R., GWINN, D., HUTCHINSON, I.,

KUSSE, B., MARMAR, E., OVERSKEI, D., PAPPAS, D., PARKER, R. R., PICKRELL, M., RICE, J., SCATURRO, L., SCHUSS, J., WEST, J., WOLFE, S., PETRASSO, R., SLUSHER, R. E., SURKO, C. M., "Study of the Energy Balance in Alcator," in Plasma Physics and Controlled Nuclear Fusion Research (Proc. 7th Int. Conf. Innsbruck, 1978) IAEA, Vienna, paper C-4 (to be published).

[14] MURAKAMI, M., NEILSON, G. H., HOWE, H. C., JERNIGAN, T. C., BATES, S. C., BUSH, C. E., COLCHIN, R. J., DUNLAP, J. L., EDMONDS, P. H., HILL, K. W., ISLER, R. C., KETTERER, H. E., KING, P. W., MCNEILL, D. W., MIHALCZO, J. T., NEIDIGH, R. V., PARÉ, V. K., SALTMARSH, M. J., WILGEN, J. B., ZURRO, B., Phys. Rev. Lett. 42 (1979) 655.

[15] POST, D. E., GOLDSTON, R. J., GRIMM, R. C., HAWRYLUK, R. J., HIRSHMAN, S. P., HSIEH, D., HULSE, R. A., JASSBY, D. L., JENSEN, R. V., MCKENNEY, A., MEADE, D. M., MIKKELSEN, D. R., OGDEN, J. M., OKABAYASHI, M., RUTHERFORD, P. H., SCHMIDT, J. A., SEIDL, F. G. P., SUCKEWER, S., TENNEY, F., MIRIN, A. A., MCCOY, M. G., KILLEEN, J., RENSINK, M. E., SHUMAKER, D. E., TARTAR, C. B., "Computational Studies of Impurity Effects, Impurity Control, and Neutral Beam Injection in Large Tokamaks," in Plasma Physics and Controlled Nuclear Fusion Research (Proc. 7th Int. Conf. Innsbruck, 1978) IAEA, Vienna, paper F-3 (to be published).

[16] EUBANK, H., GOLDSTON, R., ARUNASALEM, V., BITTER, M., BOL, K., BOYD, D., BRETZ, N., BUSSAC, J.-P., COHEN, S., COLESTOCK, P., DAVIS, S., DIMOCK, D., DYLLA, H., EFTHIMION, P., GRISHAM, L.,

HAWRYLUK, R., HILL, K., HINNOV, E., HOSEA, J., HSUAN, H., JOHNSON, D., MARTIN, G., MEDLEY, S., MERSERVEY, E., SAUTHOFF, N., SCHILLING, G., SCHIVELL, J., SCHMIDT, G., STAUFFER, F., STEWART, L., STODIEK, W., STOOKSBERRY, R., STRACHAN, J., SUCKEWER, S., TAIT, G., ULRICKSON, M., VON GOELER, S., YAMADA, M., "PLT Neutral Beam Heating Results," in Plasma Physics and Controlled Nuclear Fusion Research (Proc. 7th Int. Conf. Innsbruck, 1978) IAEA, Vienna, paper C-3 (to be published).

[17] AUDENAERDE, K., EMMERT, G. A., GORDINIER, M., SPUDNUT: A Transport Code for Neutral Atoms in Plasmas, University of Wisconsin Fusion Design Memo UWFDM-259, University of Wisconsin, Madison (1978); to be published in J. Comput. Phys.

[18] LISTER, G. G., POST, D. E., GOLDSTON, R., in Proc. 3rd Symp. on Plasma Heating in Toroidal Devices (1976) 303.

[19] ROME, J. A., CALLEN, J. D., CLARKE, J. F., Nucl. Fusion 14 (1974) 141.

[20] WIELAND, R. M., HOULBERG, W. A., MENSE, A. T., A Comparison of Beam Deposition for Three Neutral Beam Injection Codes, Oak Ridge National Laboratory Rep. ORNL/TM-6550 (1979).

[21] FOWLER, R. H., ROME, J. A., NFREYA — A Monte Carlo Beam Deposition Code for Noncircular Tokamak Plasmas, Oak Ridge National Laboratory Rep. ORNL/TM-6845 (1979).

[22] DÜCHS, D. F., FURTH, H. P., RUTHERFORD, P. H., Nucl. Fusion 12 (1972) 341.

[23] CARRERAS, B., HICKS, H. R., WADDELL, B. V., Nucl. Fusion 19 (1979) 583.

[24] DNESTROVSKII, Yu. N., KOSTOMAROV, D. P., LYSENKO, S. E., PEREVERZEV, G. V., TARASYAN, K. N., "Simulation of Discharge Dynamics in Tokamaks," in Plasma Physics and Controlled Nuclear Fusion Research (Proc. 7th Int. Conf. Innsbruck, 1978) IAEA, Vienna, paper F-1-3 (to be published).

[25] GIRARD, J. P., KHELLADI, M., MARTY, D. A., Nucl. Fusion 13 (1973) 585.

[26] STEINER, D., BECRAFT, W. R., BROWN, T. C., HOULBERG, W. A., MENSE, A. T., PENG, Y-K. M., REID, R. L., ROME, J. A., SARDELLA, C., SHANNON, T. E., SPAMPINATO, P. T., WELLS, W. M., WISEMAN, G. W., Oak Ridge TNS Program: Summary of FY 1978 Activities, Oak Ridge National Laboratory Rep. ORNL/TM-6720 (1979).

[27] HOLMES, J. A., ROME, J. A., PENG, Y-K. M., HOULBERG, W. A., LYNCH, S. J., Low Density Ignition Scenarios Using Injection Heating, Oak Ridge National Laboratory Rep. ORNL/TM-6731 (1979).

[28] MCALEES, D. G., CONN, R. W., Nucl. Fusion 14 (1974) 419.

[29] ROME, J. A., PENG, Y-K. M., HOLMES, J. A., Injection Heating Scenarios for TNS, Oak Ridge National Laboratory Rep. ORNL/TM-5931 (1977).

[30] SCOTT, S. C., SHEFFIELD, J., Scaling Studies of Beam-Heated Tokamaks, Oak Ridge National Laboratory Rep. ORNL/TM-6534 (1979).

[31] POST, D., Princeton Plasma Physics Laboratory, private communication (March 1979). Evaluation of heating requirements for INTOR with both the WHIST AND BALDUR codes shows that the results are sensitive to the model used for alpha energy deposition.

[32] BROMBERG, L., COHN, D. R., FISHER, J., Regimes of Ignited Operation, M.I.T. Plasma Fusion Center Report RR-79-3 (1979).

[33] CALLEN, J. D., ROME, J. A., Oak Ridge National Laboratory, private communication, Sherwood Meeting (1979).

Table I. Parameters for ignition plasma

| | | |
|---|---|---|
| Major radius | $R_o$ | 5.0 m |
| Minor radius | a | 1.25 m |
| Elongation | b/a | 1.6 |
| Toroidal field at $R_o$ | $B_p$ | 4.2 T |
| Plasma current | $I_p$ | 4.0 MA |

Table II. Parameters for a large power reactor

| | | |
|---|---|---|
| Major radius | $R_o$ | 10.0 m |
| Elongation | b/a | 1.6 |
| Toroidal field at $R_o$ | $B_t$ | 4.2 T |
| Beam energy ($D^o$) | $E_b$ | 150 keV |

Table III. Time-varying parameters for a large power reactor

| | Phase | | | |
|---|---|---|---|---|
| Parameter | I | II | III | IV |
| a(m) | 0.62 | 0.62-1.4 | 1.4 | 1.4-2.5 |
| $I_p$(MA) | 0.0-0.6 | 0.6-3.0 | 3.0 | 3.0-3.0 |
| t(s) | 0.0-0.1 | 0.1-2.0 | 2.0-6.0 | 6.0-12.0 |
| $P_D$(MW) | 0.0 | 0.0 | 130.0 | 0.0 |

FIGURE CAPTIONS

Fig. 1. Higher beam energy provides better penetration (near perpendicular in these cases) and more efficient heating for the same net heating power.

Fig. 2. The fraction of beam power that passes through the plasma increases with beam energy. This is a more severe problem with the small initial plasma size in the expanding radius scenario than with the full bore scenario.

Fig. 3. The ion temperature required to reach ignition increases strongly at low plasma density because of the increased anomalous electron conduction losses and the decrease in the fusion power production.

Fig. 4. The beam power required to ignite the plasma decreases strongly with increasing beam pulse length until the pulse length exceeds a few global energy confinement times.

Fig. 5. Even though the required beam power decreases with increasing beam pulse length, the total amount of required beam energy during the heating phase increases almost linearly with pulse length.

Fig. 6. The minimum power required to heat the plasma to ignition for a fixed beam pulse length is relatively insensitive to plasma density in the range $8 \times 10^{13} \leq \langle n \rangle \leq 1.2 \times 10^{14}$ cm$^{-3}$.

Fig. 7. An expanding radius scenario with 120-keV neutral deuterium beams gives heating efficiencies equivalent to a full bore scenario with 150-keV neutral deuterium beams. There is a net savings of about 20% in beam power or energy for the expanding radius scenario.

Fig. 8. The beam deposition profile is plotted as a function of time for the expanding radius scenario with 120-keV neutral deuterium beams oriented at $12^{\circ}$ from perpendicular. The uniform deposition at the end of the heating phase is indicative of H(r) for 120-keV beams in the full bore plasma.

Fig. 9. Evolution of the current density profile for the expanding radius scenario. In the first stage the current is ramped to 1 MA in 0.5 s and a skin current forms. As the plasma is expanded to full size, the current is ramped to 4 MA, and simultaneous beam heating "freezes in" the current profile.

Fig. 10. Schematic illustration of a multistaged startup of a large power-producing tokamak reactor. The values of the parameters for the example case during each phase are shown in Table III.

Fig. 11. Evolution of the ion temperature profile during the multistaged startup of a large tokamak reactor. In the final stage the beams are turned off, and fusion alpha heating is used to heat incoming cold fuel as the plasma is expanded to full size.

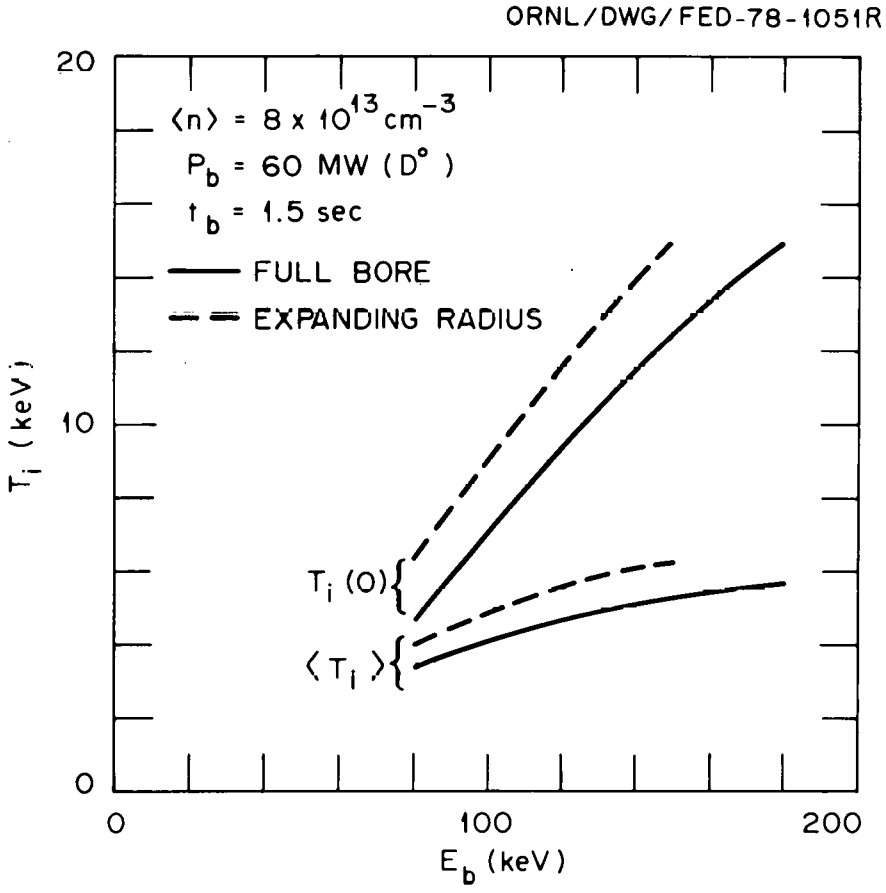
ORNL/DWG/FED-78-1051R
20
10
0
$\langle n \rangle = 8 \times 10^{13}\,cm^{-3}$
$P_b$ = 60 MW (D°)
$t_b$ = 1.5 sec
FULL BORE
EXPANDING RADIUS
$T_i$ (keV)
$T_i$ (0)
$\langle T_i \rangle$
0
100
200
$E_b$ (keV)

Figure 1

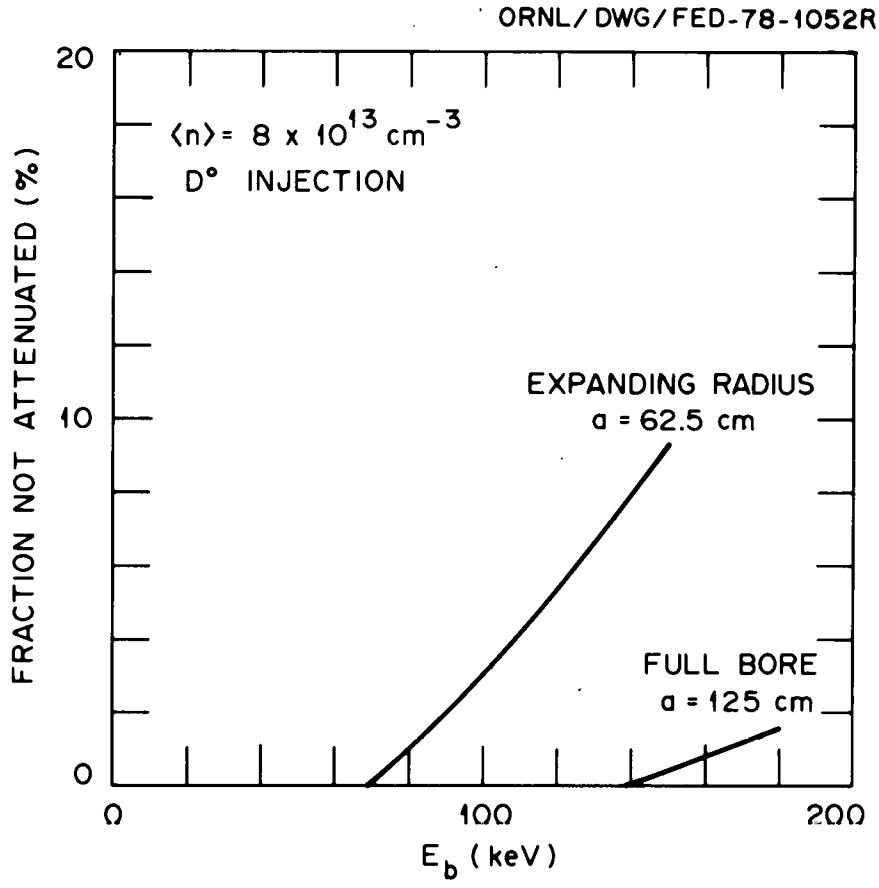
ORNL/DWG/FED-78-1052R
20
10
0
FRACTION NOT ATTENUATED (%)
⟨n⟩= 8 x 10^13 cm^-3
D° INJECTION
EXPANDING RADIUS
a = 62.5 cm
FULL BORE
a = 125 cm
0
100
200
E_b (keV)

Figure 2

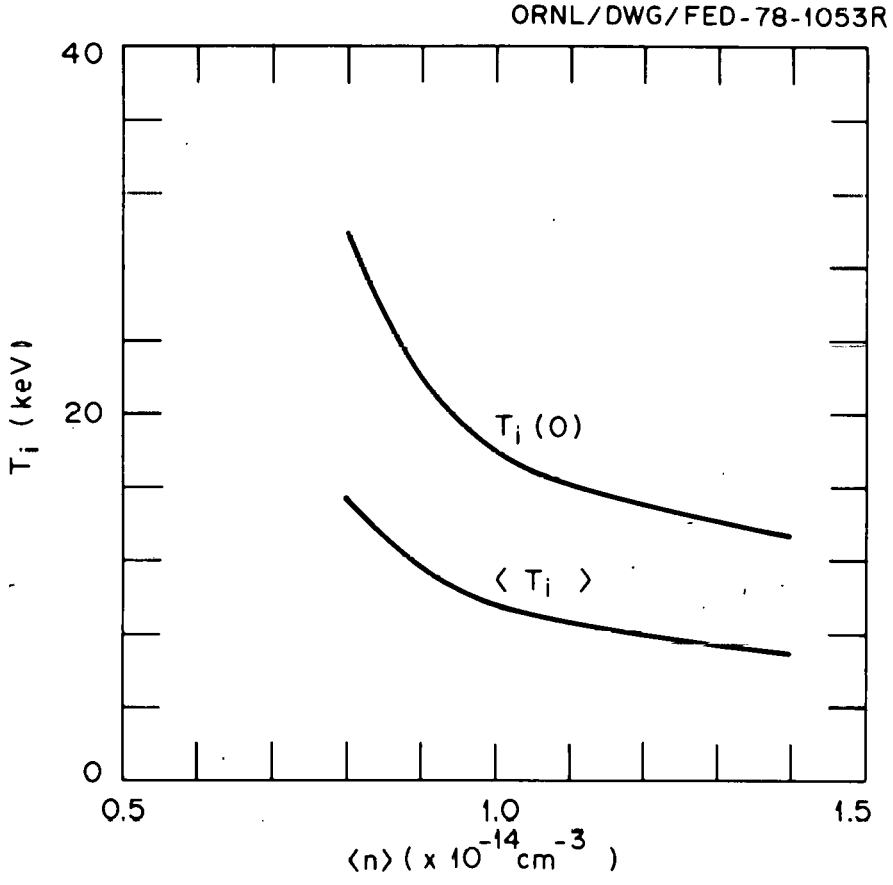


Figure 3

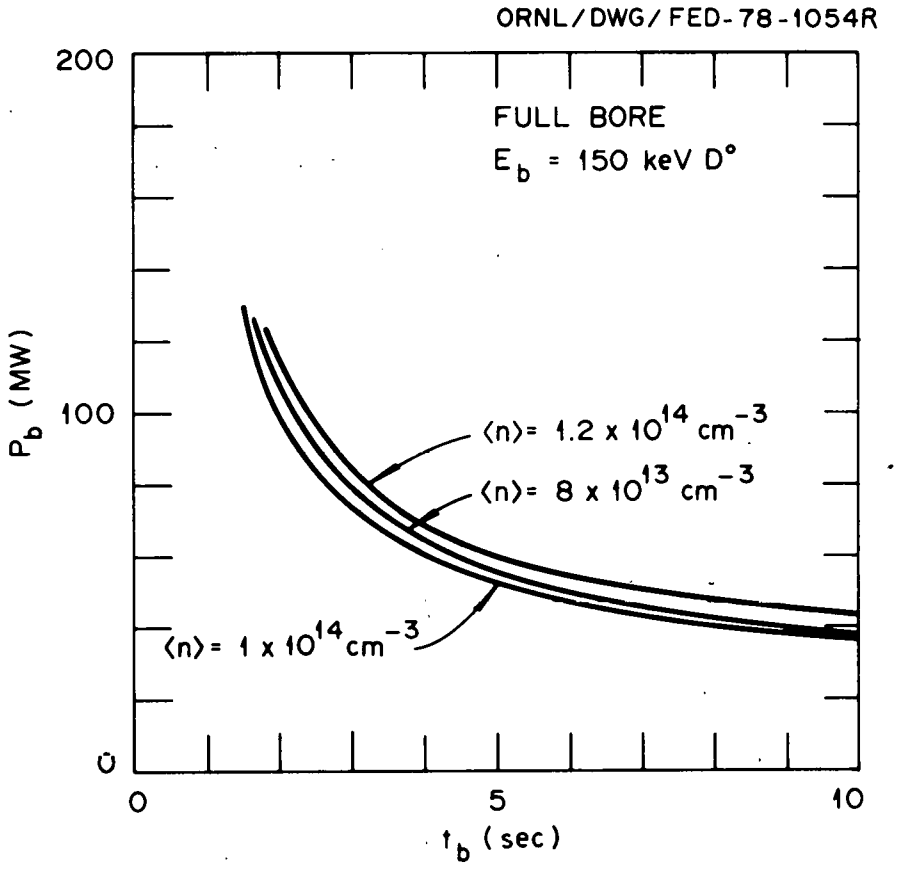
ORNL/DWG/FED-78-1054R
200
100
0
$P_b$ (MW)
FULL BORE
$E_b$ = 150 keV D°
$\langle n \rangle = 1.2 \times 10^{14}\ cm^{-3}$
$\langle n \rangle = 8 \times 10^{13}\ cm^{-3}$
$\langle n \rangle = 1 \times 10^{14} cm^{-3}$
0
5
10
$t_b$ (sec)

Figure 4

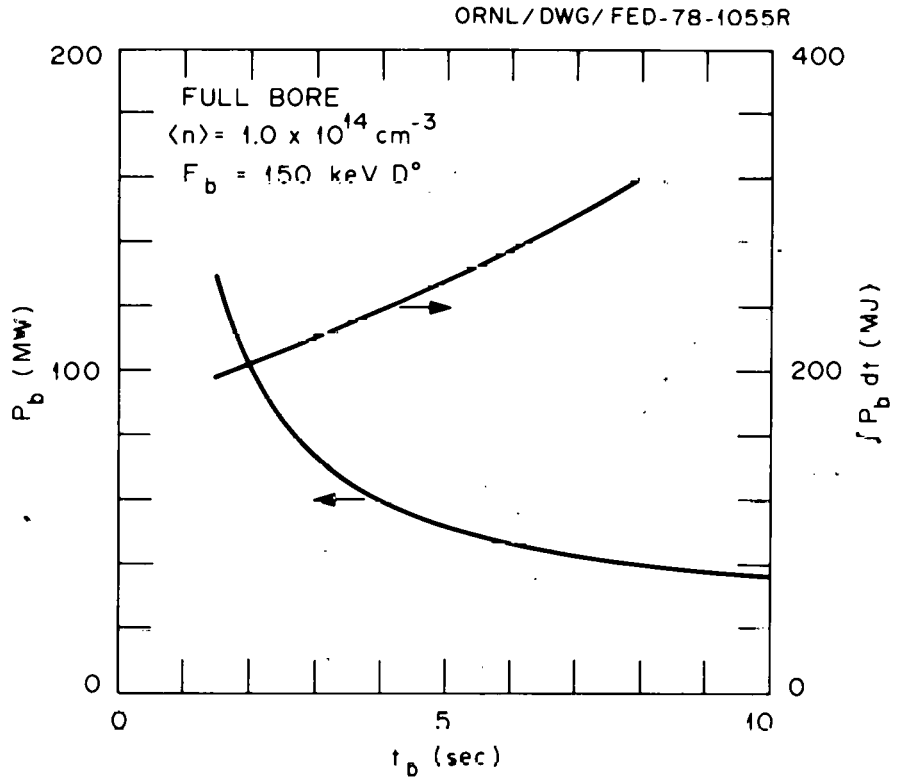
ORNL/DWG/FED-78-1055R
FULL BORE
⟨n⟩= 1.0 x 10^14 cm^-3
F_b = 150 keV D°
200
100
0
400
200
0
0
5
10
P_b (MW)
∫P_b dt (MJ)
t_b (sec)

Figure 5

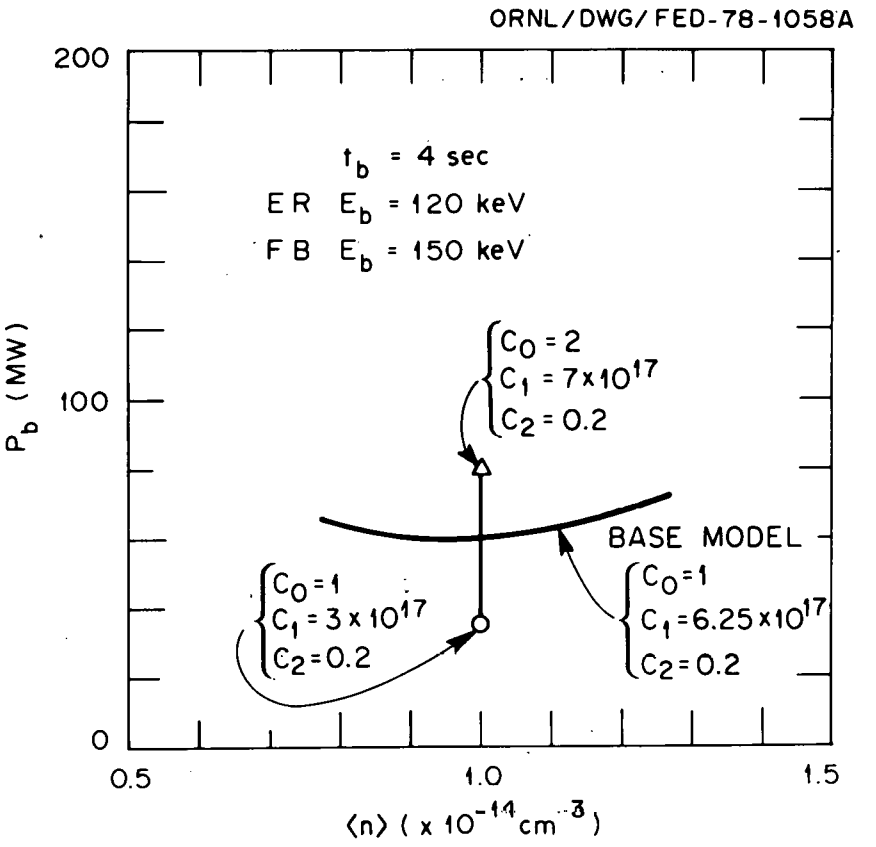
ORNL/DWG/FED-78-1058A
200
100
0
$P_b$ (MW)
$t_b$ = 4 sec
ER $E_b$ = 120 keV
FB $E_b$ = 150 keV
$C_0 = 2$
$C_1 = 7 \times 10^{17}$
$C_2 = 0.2$
BASE MODEL
$C_0 = 1$
$C_1 = 6.25 \times 10^{17}$
$C_2 = 0.2$
$C_0 = 1$
$C_1 = 3 \times 10^{17}$
$C_2 = 0.2$
0.5
1.0
1.5
$\langle n \rangle$ ( $\times 10^{-14}$ $cm^{-3}$ )

Figure 6

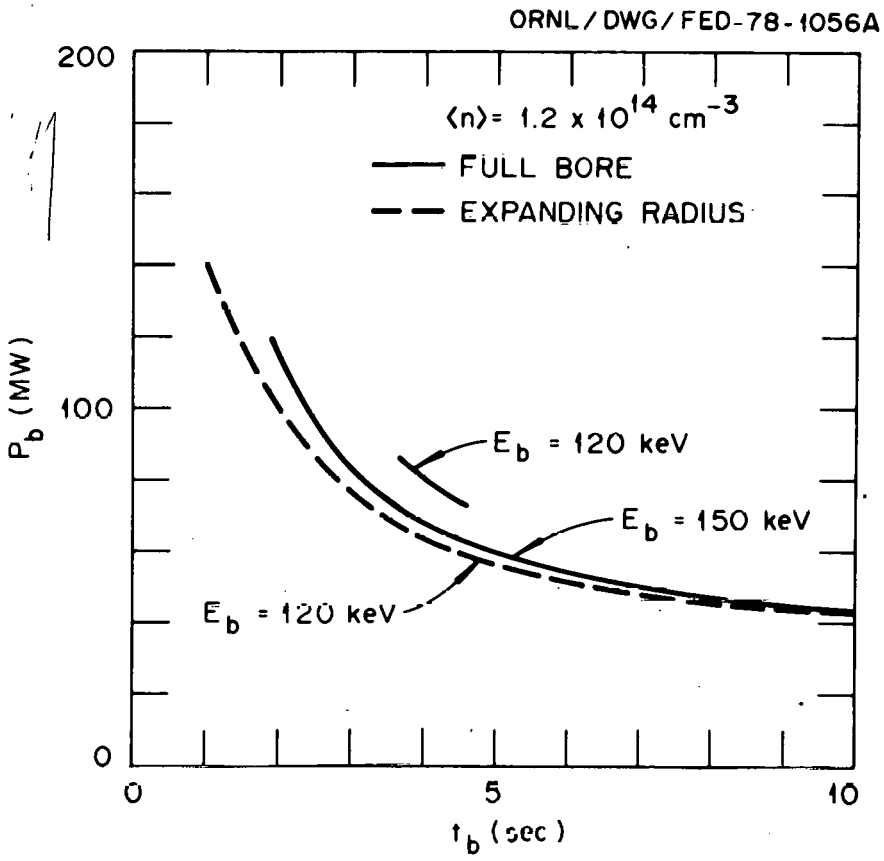
ORNL/DWG/FED-78-1056A
200
100
0
$P_b$ (MW)
$\langle n \rangle = 1.2 \times 10^{14}$ cm$^{-3}$
FULL BORE
EXPANDING RADIUS
$E_b$ = 120 keV
$E_b$ = 150 keV
$E_b$ = 120 keV
0
5
10
$t_b$ (sec)

Figure 7

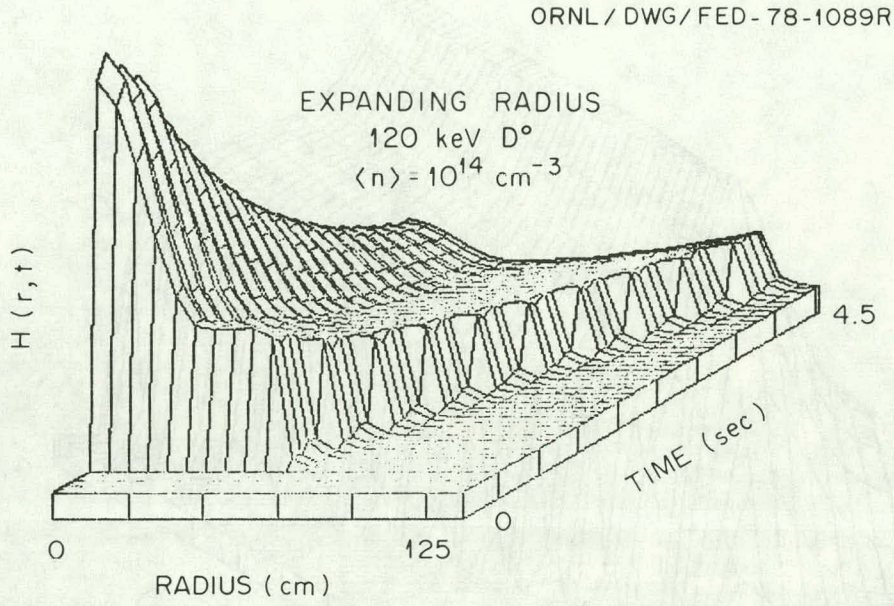
ORNL / DWG / FED - 78 - 1089R
EXPANDING RADIUS
120 keV D°
⟨n⟩ = 10^14 cm^-3
H (r, t)
4.5
TIME (sec)
0
0
125
RADIUS (cm)

Figure 8

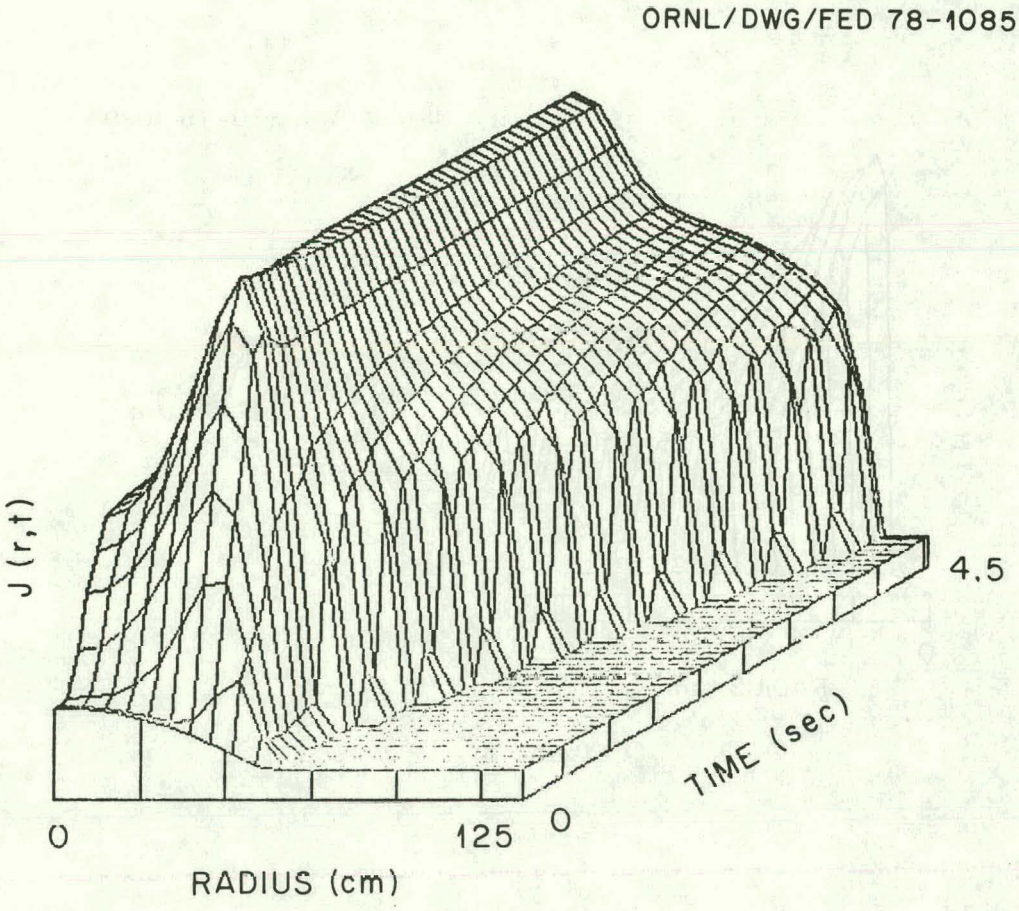


Figure 9

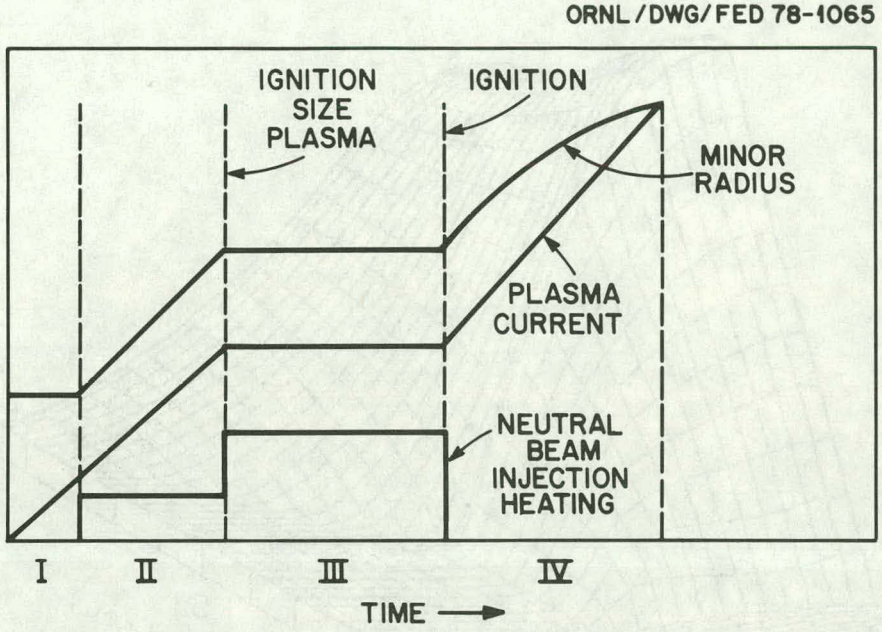
ORNL/DWG/FED 78-1065
IGNITION SIZE PLASMA
IGNITION
MINOR RADIUS
PLASMA CURRENT
NEUTRAL BEAM INJECTION HEATING
I
II
III
IV
TIME

Figure 10

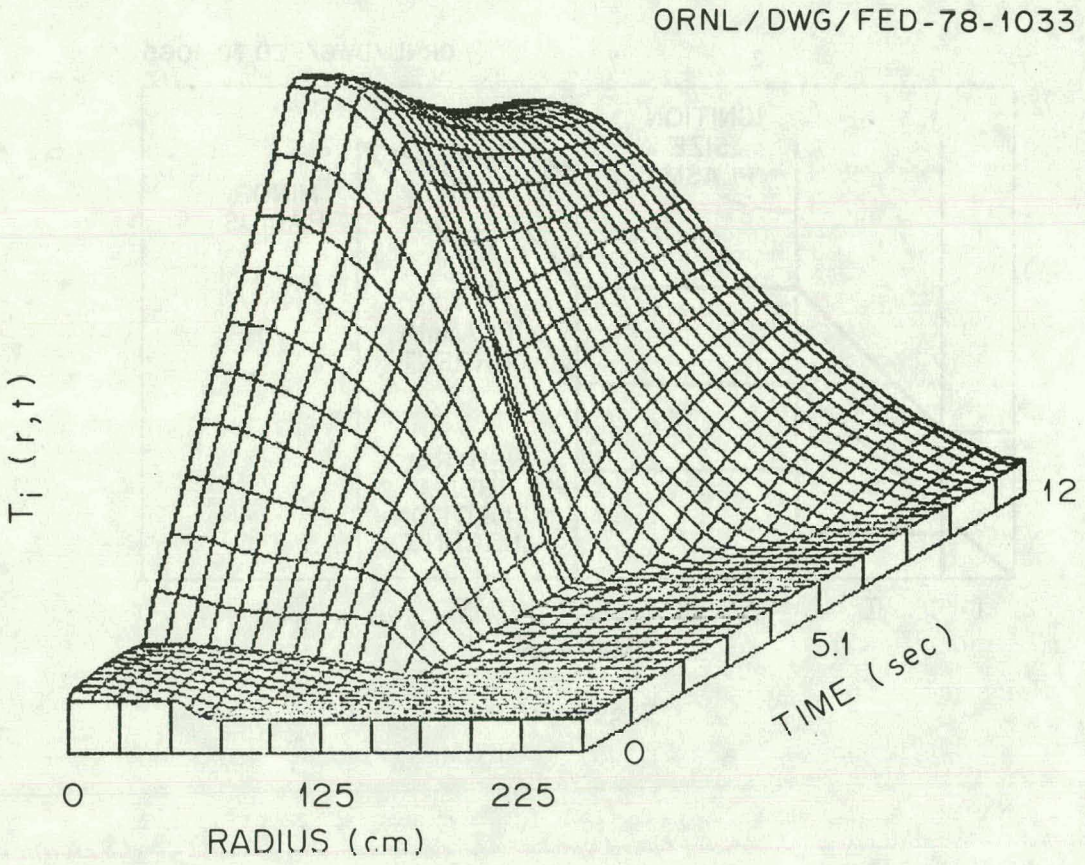


Figure 11

ORNL/TM-6730
Dist. Category UC-20 a, d, g

## INTERNAL DISTRIBUTION

1. R. G. Alsmiller
2-4. S. E. Attenberger
5. J. K. Ballou
6. W. R. Becraft
7. L. A. Berry
8. E. E. Bloom
9. A. L. Boch
10. T. G. Brown
11. E. H. Bryant
12. J. D. Callen
13. D. D. Cannon
14. R. J. Colchin
15. R. A. Dory
16. J. L. Dunlap
17. J. T. Hogan
18-27. W. A. Houlberg
28. M. S. Lubell
29. J. W. Lue
30. O. B. Morgan
31. L. W. Nelms
32. Y-K. M. Peng
33. R. L. Reid
34. J. A. Rome
35. M. W. Rosenthal
36. R. T. Santoro
37. C. Sardella
38. J. L. Scott
39. T. E. Shannon
40. J. Sheffield
41-60. D. Steiner
61. N. A. Uckan
62. J. S. Watson
63. W. M. Wells
64. F. W. Wiffen
65. G. W. Wiseman
66. H. T. Yeh
67-68. Central Research Library
69-70. Fusion Energy Division Library
71. Fusion Energy Division Communications Center
72-73. Laboratory Records Department
74. Laboratory Records, ORNL-RC
75. ORNL Patent Office
76. Document Reference Section

## EXTERNAL DISTRIBUTION

77. R. E. Aronstein, Bechtel, P.O. Box 3965, San Francisco, CA 94119
78. D. J. Anthony, General Electric Co., Bldg. 23, Rm. 290, 1 River Rd., Schenectady, NY 12345
79. J. E. Baublitz, Office of Fusion Energy, G-234, Department of Energy, Washington, DC 20545
80. D. S. Beard, Office of Fusion Energy, G-234, Department of Energy, Washington, DC 20545
81. G. Benedict, Department of Energy, Oak Ridge Operations, P.O. Box E, Oak Ridge, TN 37830
82. Bibliothek, Max-Planck Institute für Plasmaphysik, 8046 Garching bei München Federal Republic of Germany
83. Bibliothèque, Service du Confinement des Plasmas, C.E.A., B.P. No. 6, 92, Fontenay-aux-Roses (Seine), France
84. S. L. Bogart, Science Applications, Inc., 8400 Westpark Drive, McClean, VA 22102
85. R. Boom, University of Wisconsin, Madison, WI 53706
86. R. T. Botwin, Grumman Aerospace Corp., Bethpage, NY 11714
87. R. N. Cherdack, Burns and Roe, Inc., 283 Highway 17, Paramus, NJ 07652
88. L. Cheung, Department of Electronics, University Science Center, The Chinese University of Hong Kong, Shatin, N.T., Hong Kong

89. J. F. Clarke, Office of Fusion Energy, G-234, Department of Energy, Washington, DC 20545
90. F. E. Coffman, Office of Fusion Energy, G-234, Department of Energy, Washington, DC 20545
91. D. Cohn, Massachusetts Institute of Technology, Cambridge, MA 02139
92. J. W. Coursen, Grumman Aerospace Corp., Bethpage, NY 11714
93. J. G. Crocker, EG & G Idaho, Idaho National Engineering Laboratory, P.O. Box 1625, Idaho Falls, ID 83401
94. CTR Library, c/o Alan F. Haught, United Technologies Research Laboratory, East Hartford, CT 06108
95. CTR Reading Room, c/o Allan N. Kaufman, Physics Department, University of California, Berkeley, CA 94720
96. Library, Culham Laboratory, Abingdon, Oxon, OX14, 3DB, United Kingdom
97. J. N. Davidson, School of Nuclear Engineering, Georgia Institute of Technology, Atlanta, GA 30332
98. N. A. Davies, Offfice of Fusion Energy, G-234, Department of Energy, Washington, DC 20545
99. H. W. Deckman, Advanced Energy Systems Laboratory, Government Research Laboratories, Exxon Research and Engineering Co., P.O. Box 8, Linden, NJ 07036
100. Documentation S.I.G.N., Département de la Physique du Plasma et de la Fusion Controlée, Association EURATOM-CEA sur la Fusion, Centre d'Études Nucléaires, B. P. 85, Centre du Tri, 38041 Grenoble, Cedex, France
101. W. R. Ellis, Office of Fusion Energy, G-234, Department of Energy, Washington, DC 20545
102. G. A. Emmert, Nuclear Engineering Department, University of Wisconsin, Madison, WI 53706
103. A. Favale, Grumman Aerospace Corp., Bethpage, NY 11714
104. J. J. Ferrante, Large Coil Program, Bldg. 2-708, General Electric Co., 1 River Rd., Schenectady, NY 12345
105. F. Fickett, National Bureau of Standards, Boulder, CO 80302
106. C. A. Flanagan, Westinghouse Electric Corp., Fusion Power Systems, P.O. Box 10864, Pittsburgh, PA 15236
107. H. K. Forsen, Exxon Nuclear Co., Inc., 777 106th Ave., Bellevue WA 98009
108. J. W. French, EBASCO Services, Inc., Princeton University, P.O. 451, Princeton, NJ 08540
109. G. M. Fuller, McDonnell-Douglas, Dept. E-450, Bldg. 10613, Rm. 370, St. Louis, MO 63166
110. H. P. Furth, Princeton Plasma Physics Laboratory, Princeton University, P.O. Box 451, Princeton, NJ 08540
111. A. Gaines, Combustion Engineering, 100 Prospect Hill Rd., Windsor, CT 06095
112. A. Gibson, Culham Laboratory, Abingdon, Oxon, OX14 3DB, United Kingdom
113. R. W. Gould, Mail Stop 116-81, California Institute of Technology, Pasadena, CA 91125
114. E. Gregory, Airco Inc., Murray Hill, NJ 07974
115. D. S. Hackley, Large Coil Program, General Dynamics-Convair Division, P.O. Box 80847, San Diego, CA 92138

116. R. Hancox, Culham Laboratory, Abingdon, Oxon OX14 3DB, United Kingdom
117. C. R. Head, Office of Fusion Energy, G-234, Department of Energy, Washington, DC 20545
118. C. Henning, Lawrence Livermore Laboratory, P.O. Box 808, Livermore, CA 94550
119. R. L. Hirsch, Exxon Research and Engineering Co., P.O. Box 101, Florham Park, NJ 07932
120. A. Hsu, Office of Fusion Energy, G-234, Department of Energy, Washington, DC 20545
121. R. A. Huse, Manager, Research and Development, Public Service Gas and Electric Company, 80 Park Place, Newark, NJ 07101
122. V. E. Ivanov, Physical-Technical Institute of the Ukranian Academy of Sciences, 310108 Kharkov, U.S.S.R.
123. D. L. Jassby, Princeton Plasma Physics Laboratory, Princeton University, P.O. Box 451, Princeton, NJ 08540
124. A. Kadish, Office of Fusion Energy, G-234, Department of Energy, Washington, DC 20545
125. Y. Kiwamoto, Research Institute for Energy Materials, Yokohama National University, Yokohama 232, Japan
126. L. M. Kovrizhnykh, Lebedev Institute of Physics, Academy of Sciences of the U.S.S.R., Leninsky Prospect 53, Moscow, U.S.S.R.
127. D. L. Kummer, McDonnell-Douglas Astronautics Co., East, P.O. Box 516, St. Louis, MO 63166
128. G. Laval, Groupe de Physique Théorique, Ecole Polytechnique, 91 Palaiseau, Paris, France
129. Library, Centre de Recherches en Physique des Plasma, 21 Avenue des Bains, 1007, Lausanne, Switzerland
130. Library, FOM-Institut voor Plasma — Fysica, Rijnhuizen, Jutphaas, Netherlands
131. Library, Institute for Plasma Physics, Nagoya University, Nagoya, Japan 464
132. Library, International Centre for Theoretical Physics, Trieste, Italy
133. Library, Laboratorio Gas Ionizzati, Frascati, Italy
134. D. G. Lominadze, Academy of Sciences of the Georgian S.S.R., 8 Dzerzhinski St., 38004, Tbilisi, U.S.S.R.
135. O. P. Manley, Office of Fusion Energy, G-234, Department of Energy, Washington, DC 20545
136. D. G. McAlees, Manager, ETF Systems Interface, Exxon Nuclear Co., Inc., Research and Technical Center, 2955 George Washington Way, Richland, WA 99352
137. J. E. McCune, School of Engineering, Department of Aeronautics and Astronautics, Bldg. 37-391, Massachusetts Institute of Technology, Cambridge, MA 02139
138. V. A. Maroni, Argonne National Laboratory, 9700 South Cass Ave., Argonne, IL 60439
139. D. M. Meade, Princeton Plasma Physics Laboratory, Princeton, University, P.O. Box 451, Princeton, NJ 08540
140-149. A. T. Mense, Subcommittee on Energy Research and Production, B-374, Rayburn House Office Building, Washington, DC 20515

150. C. L. Mercier, Service du Theorie des Plasmas, Centre d'Études Nucléaires, Fontenay-aux-Roses (Seine), France
151. R. L. Miller, General Atomic Co., P.O. Box 81608, San Diego, CA 92138
152. R. N. Kostoff, Room 509, Office of Fusion Energy Research, Department of Energy, 401 First St., N.W., Washington, DC 20545
153. M. R. Murphy, Office of Fusion Energy, G-234, Department of Energy, Washington, DC 20545
154. J. G. Murray, Princeton Plasma Physics Laboratory, Princeton University, P.O. Box 451, Princeton, NJ 08540
155. D. Pfirsch, Institute for Plasma Physics, 8046 Garching bei München, Federal Republic of Germany
156. Plasma Physics Group, Department of Engineering Physics, Australian National University, P.O. Box 4, Canberra A.C.T. 2600, Australia
157. L. K. Price, Department of Energy, Oak Ridge Operations, P.O. Box E, Oak Ridge, TN 37830
158. J. M. Rawls, General Atomic Co., P.O. Box 81608, San Diego, CA 92138
159. P. Reardon, Princeton Plasma Physics Laboratory, Princeton University, P.O. Box 451, Princeton, NJ 08540
160. T. Reuther, Office of Fusion Energy, G-234, Deparment of Energy, Washington, DC 29545
161. M. Roberts, Office of Fusion Energy, G-234, Department of Energy, Washington, DC 20545
162. A. Rogister, Institute for Plasma Physics, KFA, Postfach 1913, D-5170, Jülich 1, Federal Republic of Germany
163. D. J. Rose, Department of Nuclear Engineering, Massachusetts Institute of Technology, Cambridge, MA 02139
164. M. N. Rosenbluth, School of Natural Sciences, Princeton University, P.O. Box 451, Princeton, NJ 08540
165. C. Rosner, Intermagnetics General Corp., Charles Industrial Park, New Karner Rd., Guilderland, NY 12084
166. W. Sadowski, Office of Fusion Energy, G-234, Department of Energy, Washington, DC 20545
167. P. H. Sager, Jr., General Atomic Co., P.O. Box 81608, San Diego, CA 92138
168. G. Schilling, Princeton Plasma Physics Laboratory, Princeton University, P.O. Box 451, Princeton, NJ 08540
169. V. D. Shafranov, I. V. Kurchatov Institute of Atomic Energy, 46 Ulitsa Kurchatova, P.O. Box 3402, Moscow, U.S.S.R.
170. Z. M. Shapiro, Westinghouse Electric Corp., Fusion Power Systems Department, P.O. Box 10864, Pittsburgh, PA 15236
171. C. Siegel, Tennessee Valley Authority, 1360 Commerce Union Bank Bldg., Chattanooga, TN 37401
172. Yu. S. Sigov, Institute of Applied Mathematics of the U.S.S.R. Academy of Sciences, Miuskaya, Sq. 4, Moscow A-47, U.S.S.R.
173. A. Simon, University of Rochester, Rochester, NY 14627
174. W. M. Stacey, Jr., School of Nuclear Engineering, Georgia Institute of Technology, Atlanta, GA 30332
175. J. Stekly, Magnetic Corp. of America, 179 Bear Hill Rd., Waltham, MA 02154

176. L. D. Stewart, Princeton Plasma Physics Laboratory, Princeton University, P.O. Box 451, Princeton, NJ 08540
177. C. Taylor, Controlled Thermonuclear Research, Mail Code L-382, Lawrence Livermore Laboratory, P.O. Box 808, Livermore, CA 94550
178. J. B. Taylor, Culham Laboratory, U.K. Atomic Energy Authority, Abingdon, Oxon, OX14 3DB, United Kingdom
179. Thermonuclear Library, Japan Atomic Energy Research Institute, Tokai, Naka, Ibaraki, Japan
180. F. Thomas, Grumman Aerospace Corp., Bethpage, NY 11714
181. T. C. Varljen, Westinghouse Electric Corp., Fusion Power Systems, P.O. Box 10864, Pittsburgh, PA 15236
182. F. Verdaguer, Director, Division of Fusion, Junta de Energia Nuclear, Madrid 3, Spain
183. S. S. Waddle, Department of Energy, Oak Ridge Operations, P.O. Box E, Oak Ridge, TN 37830
184. J. Willis, Office of Fusion Energy, G-234, Department of Energy, Washington, DC 20545
185. W. Wilkes, Mound Laboratories, Miamiburg, OH 45432
186. H. H. Woodson, Department of Electrical Engineering, University of Texas, Austin, TX 78712
187. W. W. Withee, Energy Systems, General Dynamics-Convair Division, P.O. Box 80847, San Diego, CA 92138
188. S. Yoshikawa, Princeton Plasma Physics Laboratory, Princeton University, P.O. Box 451, Princeton, NJ 08540
189. J. L. Young, Large Coil Program, Westinghouse Electric Corp., 1310 Beulah Road, Pittsburgh, PA 15235
190. E. Ziurys, Office of Fusion Energy, G-234, Department of Energy, Washington, DC 20545
191. K. Zwilsky, Office of Fusion Energy, G-234, Department of Energy, Washington, DC 20545
192. Office of Assistant Manager, Energy Research and Development, Department of Energy, Oak Ridge Operations, P.O. Box E, Oak Ridge, TN 37830

193-437. Given distribution as shown in TID-4500, Magnetic Fusion Energy (Distribution Category UC-20 a, d, g: Plasma Systems, Fusion Systems, and Theoretical Plasma Physics)